Journal of Non-Newtonian Fluid Mechanics, 22 (1987) 289–307
Elsevier Science Publishers B.V., Amsterdam – Printed in The Netherlands

FLOW OF K-BKZ FLUIDS BETWEEN PARALLEL PLATES ROTATING ABOUT DISTINCT AXES: SHEAR THINNING AND INERTIAL EFFECTS

M.V. BOWER

Department of Mechanical Engineering, University of Alabama in Huntsville, Huntsville, AL 35805 (U.S.A.)

A.S. WINEMAN

Department of Mechanical Engineering and Applied Mechanics, University of Michigan, Ann Arbor, MI 48109 (U.S.A.)

K.R. RAJAGOPAL

Department of Mechanical Engineering, University of Pittsburgh, Pittsburgh, PA 15261 (U.S.A.)

(Received May 28, 1986)

Summary

It has been shown that for any simple fluid, a flow field of the form $u = -\Omega[y - g(z)]$, $v = \Omega[x - f(z)]$, $w = 0$, which is appropriate for modeling the flow in a orthogonal rheometer, is dynamically possible. The functions $f(z)$ and $g(z)$ depend on the choice of constitutive equation. In the present paper, these are calculated for a class of K-BKZ fluids which exhibit shear thinning. The results are then used to study the interaction of shear thinning and inertial effects on the flow field in an orthogonal rheometer.

1. Introduction

The flow of viscoelastic fluids in an orthogonal rheometer has been studied by various authors (cf. Maxwell and Chartoff [1], Blyler and Kurtz [2], Goldstein and Schowalter [3] and others). A more complete list of references can be found in [4]. The early investigations primarily ignored the inertial effects. Abbot and Walters [5] were the first to incorporate the inertial effects and they obtained an exact solution in the case of the classical linearly viscous fluid. In the case of a more general viscoelastic

0377-0257/87/$03.50

fluid, they employed a perturbation analysis assuming the offset between the axes to be small. In the case of an incompressible fluid of second grade (cf. Truesdell and Noll [6]), Rajagopal [7] has included inertial effects and has established an exact solution.

Recently, Rajagopal [4] showed that for any simple fluid, the flow field

$$u = -\Omega[y - g(z)],$$

$$v = \Omega[x - f(z)],$$

$$w = 0,$$

which is appropriate for modeling the flow in an orthogonal rheometer, is dynamically possible.* In particular, Rajagopal [4] showed that the velocity field is characterized by the two functions $f(z)$, $g(z)$ which satisfy a system of non-linear second order differential equations and thus the no slip boundary conditions are sufficient for determinacy. The form of the differential equations depends on the choice of the constitutive equations. Rajagopal and Wineman [9] used this result to study the effect of inertia on the flow of a special subclass of K-BKZ fluids in an orthogonal rheometer. This subclass is a generalization of Lodge's rubber-like liquid [10] and exhibits no shear thinning. Rajagopal and Wineman [9] obtained an exact analytic solution for this case, which makes it one of the few known non-trivial exact solutions involving the flow of a fluid characterized by an integral model. They showed that large deviations from the classical non-inertial solutions would occur if the rotation rates or the plate separation are sufficiently large.

In the present paper, the earlier study of Rajagopal and Wineman [9] is extended to a more general class of K-BKZ fluids which exhibits shear thinning. This work is motivated by several considerations. First, the problem under consideration highlights the interplay between shear thinning and inertia in a complicated flow. Secondly, since the corresponding equations for $f(z)$ and $g(z)$ require a numerical method of solution, this represents a numerical simulation of a flow of a viscoelastic fluid represented by an integral model. In distinction from other numerical work, the present paper uses a semi-inverse technique in which the velocity field is specified *a priori*. When numerical difficulties arise, they can be traced to the development of a boundary layer at the plate of the orthogonal rheometer, or to unusual properties of the constitutive equation.

A brief treatment of the kinematics and the equations of motion is presented in section 2. The particular choice of a shear thinning K-BKZ fluid is introduced in section 3. Two material property functions arise which

* Essentially the same result has been established independently by Goddard [8].

are analogous to the real and imaginary parts of the complex modulus, but which depend on the shear strain amplitude. The boundary value problem is defined in section 4. Also in this section, expressions are developed for the error when inertia is neglected in the formula for finding the material properties from the experimental data. The computation of the material property functions, and their general characteristics, are discussed in section 5. In section 6, a numerical method for solving the boundary value problem is outlined. Numerical results are presented and discussed in section 7 using data which are typical in experimental applications of the orthogonal rheometer.

A study of this problem has also been carried out by Rajagopal et al. [11]. They use another class of integral models which exhibit shear thinning. However, the goals of the study and the method of solving the governing equations are quite different. Their interest is in the qualitative properties of the solution of the governing equations, whereas the interest here is in a detailed study of the interaction of shear thinning and inertia and the determination of corrections due to inertia.

2. Kinematics and governing equations

An idealized orthogonal rheometer is shown in Fig. 1. The plate separation is $2h$, the distance between the axes of rotation is $2a$ and the angular

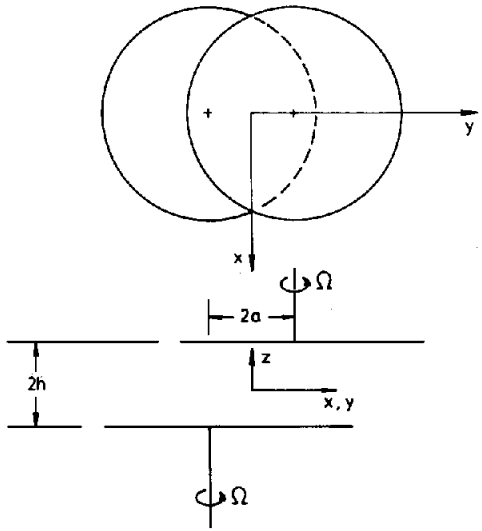

Fig. 1. Schematic drawing of an orthogonal rheometer.

velocity of the plates is Ω. The coordinate system is as shown. Rajagopal [4] assumed a velocity field of the form

$$u = -\Omega(y - g(z)), \qquad v = \Omega(x - f(z)), \qquad w = 0, \tag{2.1}$$

where u, v and w are the x, y and z components of velocity, respectively. In this velocity field, the fluid layer at $z =$ constant undergoes a rigid body rotation about the point $(f(z), g(z))$. The relative motion, relative deformation gradient and other quantities of kinematic importance can be obtained from (2.1) by a lengthy but straightforward computation. The relevant results for the fluid model under consideration will be presented in the next section.

For this motion, Rajagopal [4] showed that the stress $\boldsymbol{T}$ in an incompressible simple fluid can be expressed as

$$\boldsymbol{T} = -p\boldsymbol{I} + \boldsymbol{R}(\boldsymbol{A}_1, \boldsymbol{A}_2), \tag{2.2}$$

where p is the indeterminate scalar arising from the constraint of incompressibility and $\boldsymbol{A}_1$ and $\boldsymbol{A}_2$ are the first two Rivlin–Ericksen tensors [6]. Since the latter depend on $f'(z)$ and $g'(z)$ where the prime denotes differentiation with respect to z, (2.2) can be rewritten as

$$\boldsymbol{T} = -p\boldsymbol{I} + \boldsymbol{R}(f', g'). \tag{2.3}$$

Let (2.1) and (2.3) be substituted into the equations of motion, and let it be assumed that the body force is conservative and derivable from a potential. After operating on the equations of motion by the curl operator in order to eliminate p, one obtains the equations

$$\frac{\mathrm{d}R_{13}}{\mathrm{d}z} = \rho\Omega^2 f(z) + q \tag{2.4}$$

and

$$\frac{\mathrm{d}R_{23}}{\mathrm{d}z} = \rho\Omega^2 g(z) + s, \tag{2.5}$$

where q and s are constants. The existence of asymmetric solutions associated with $q \neq 0$ and $s \neq 0$ and the qualitative properties of eqns. (2.4) and (2.5) are discussed in [11] for a class of integral models. In fact, Berker has exhibited the existence of a two parameter family of asymmetric solutions even in the case of a Navier–Stokes fluid [12]. An expression for p can be easily obtained and is presented in [9]. In this paper we shall study the case $q = 0$ and $s = 0$, which implies mid-plane symmetry.

Equations (2.4) and (2.5) are two non-linear ordinary differential equations for $f(z)$ and $g(z)$. The appropriate boundary conditions arise from the adherence conditions on the upper and lower plates of the orthogonal

rheometer. Since the centers of rotation of the plates at $z = \pm h$ are at $(f(\pm h),\ g(\pm h)) = (0,\ \pm a)$, the boundary conditions on $f(z)$ and $g(z)$ are

$$f(-h) = f(h) = 0, \qquad g(-h) = -a, \qquad g(h) = a. \tag{2.6}$$

Due to the symmetry of flow about $z = 0$, it is sufficient to consider only the region $0 \leqslant z \leqslant h$. Alternate boundary conditions for the problem are then

$$f(0) = 0, \qquad g(0) = 0, \qquad f(h) = 0, \qquad g(h) = a. \tag{2.7}$$

3. Fluid model

We shall study the flow of a K-BKZ fluid (cf. Kaye [13], Bernstein, Kearsley and Zapas [14]) in the orthogonal rheometer. In order to present this framework, let $\boldsymbol{F}_t(\tau)$ denote the gradient of the particle coordinate $x(\tau)$ at time τ with respect to the coordinate $x(t)$ at time t, i.e. in a Cartesian coordinate system, $F_t(\tau)_{ij} = \partial x_i(\tau)/\partial x_j(t)$. The strain tensor $\boldsymbol{C}_t(\tau)$ is defined by

$$\boldsymbol{C}_t(\tau) = \boldsymbol{F}_t^{\mathrm{T}}(\tau)\boldsymbol{F}_t(\tau), \tag{3.1}$$

and its principal invariants are

$$I_1(t,\ \tau) = \operatorname{tr} \boldsymbol{C}_t^{-1}(\tau),$$
$$I_2(t,\ \tau) = \operatorname{tr} \boldsymbol{C}_t(\tau). \tag{3.2}$$

A K-BKZ fluid is characterized by the stored energy potential function U which depends on I_1, I_2 and $t - \tau$, i.e.

$$U = U(I_1,\ I_2,\ t - \tau), \tag{3.3}$$

and the stress $\boldsymbol{T}$ is given in terms of U by

$$\boldsymbol{T} = -p\boldsymbol{I} + 2\int_{-\infty}^{t} \left\{U_1 \boldsymbol{C}_t^{-1}(\tau) - U_2 \boldsymbol{C}_t(\tau)\right\} \mathrm{d}\tau, \tag{3.4}$$

where

$$U_1 = \partial U/\partial I_1, \qquad U_2 = \partial U/\partial I_2. \tag{3.5}$$

For the motion based on (2.1),

$$I_1 = I_2 = 3 + 2(1 - \cos\Omega(t - \tau))\kappa^2$$
$$\equiv I(\Omega(t - \tau),\ \kappa) \tag{3.6}$$

where

$$\kappa^2 = (f')^2 + (g')^2. \tag{3.7}$$

The fluid motion is such that each material particle moves on a circular path in the plane $z = \text{const.}$, and undergoes an oscillatory shear strain

history. The amplitude of the shear strain is proportional to κ. The shear stress components $T_{xz} = R_{13}$, $T_{yz} = R_{23}$ in eqns. (2.4) and (2.5) are given by

$$T_{xz} = B(\kappa, \Omega)f'(z) + A(\kappa, \Omega)g'(z), \tag{3.8}$$

$$T_{yz} = -A(\kappa, \Omega)f'(z) + B(\kappa, \Omega)g'(z), \tag{3.9}$$

where

$$A(\kappa, \Omega) = 2\int_0^\infty \tilde{U}(I(\Omega s, \kappa);\ s) \sin \Omega s \, ds, \tag{3.10}$$

$$B(\kappa, \Omega) = 2\int_0^\infty \tilde{U}(I(\Omega s, \kappa);\ s)(1 - \cos \Omega s) \, ds \tag{3.11}$$

and

$$\tilde{U}(I, s) = U_1(I, I, s) + U_2(I, I, s). \tag{3.12}$$

The particular choice for U will be that developed by Wagner [15] from experimental data on shear flows. This model predicts shear thinning response in steady shear flow experiments. It is given by

$$U_1 = 0, \qquad U_2 = -\frac{1}{2}\frac{dG(s)}{ds} \exp\left(-n\sqrt{I_2 - 3}\right), \tag{3.13}$$

where $G(s)$ is the shear stress relaxation function in the linear viscoelastic regime and n is an experimentally determined constant. For low density polyethylene melts, $n = 0.29$.

Substitution of (3.13) into (3.10)–(3.12) gives

$$A(\kappa, \Omega) = -\int_0^\infty \dot{G}(s) \exp\left(-n\kappa\sqrt{2(1 - \cos \Omega s)}\right) \sin \Omega s \, ds, \tag{3.14}$$

$$B(\kappa, \Omega) = -\int_0^\infty \dot{G}(s) \exp\left(-n\kappa\sqrt{2(1 - \cos \Omega s)}\right)(1 - \cos \Omega s) \, ds. \tag{3.15}$$

Note that

$$\lim_{\kappa \to 0} A(\kappa, \Omega) = -\int_0^\infty \dot{G}(s) \sin \Omega s \, ds = G_2(\Omega), \tag{3.16}$$

$$\lim_{\kappa \to 0} B(\kappa, \Omega) = -\int_0^\infty \dot{G}(s)(1 - \cos \Omega s) \, ds = G_1(\Omega), \tag{3.17}$$

where $G_1(\Omega)$ and $G_2(\Omega)$ are the real and imaginary components of the complex modulus in linear viscoelastic response.

The results in [9] correspond to the case in which $n = 0$ in (3.14) and (3.15). In order to relate the results in the present work to those in [9], the relaxation function $G(s)$ used in [9] will also be used here. Thus, $G(s)$ is taken as that for a 19.3% solution of polyisobutylene in cetane for which experimental stress relaxation data were provided by L. Zapas of the

TABLE 1

Stress relaxation data for a 19.3% solution of polyisobutylene in cetane ($\rho = 900$ kg/m^3)

Time (s)	Relaxation function value $G(t)$ (Pa)
0.0	800.0
0.2	562.0
0.5	340.0
1.0	213.0
2.5	86.0
5.0	38.0
10.0	14.6

National Bureau of Standard [16]. The data are listed in Table 1. The value $G(0) = 800$ N/m^2 was obtained by extrapolation. For $s \geqslant 10$ seconds, $G(s)$ was approximated by a linear extrapolation to zero. A natural cubic spline was fitted to the data in Table 1 in order to generate a representation for $G(s)$, $0 \leqslant s \leqslant 10$.

4. The boundary value problem

The system of equations for $f(z)$ and $g(z)$ is obtained by substituting (3.8) and (3.9) into (2.4) and (2.5), in which $q = s = 0$. This gives,

$$\frac{\mathrm{d}}{\mathrm{d}z}\left\{B(\kappa, \Omega)\frac{\mathrm{d}f}{\mathrm{d}z} + A(\kappa, \Omega)\frac{\mathrm{d}g}{\mathrm{d}z}\right\} = \rho\Omega^2 f, \tag{4.1}$$

$$\frac{\mathrm{d}}{\mathrm{d}z}\left\{-A(\kappa, \Omega)\frac{\mathrm{d}f}{\mathrm{d}z} + B(\kappa, \Omega)\frac{\mathrm{d}g}{\mathrm{d}z}\right\} = \rho\Omega^2 g, \tag{4.2}$$

where κ, A and B are given by (3.7), (3.14) and (3.15), respectively. The boundary conditions are stated in (2.7).

Let t_x and t_y denote the x and y components of the tractions on the upper layer of fluid. By (3.4), (3.8) and (3.9)

$$t_x = B(\bar{\kappa}, \Omega)f'(h) + A(\bar{\kappa}, \Omega)g'(h), \tag{4.3}$$

$$t_y = -A(\bar{\kappa}, \Omega)f'(h) + B(\bar{\kappa}, \Omega)g'(h), \tag{4.4}$$

where

$$\bar{\kappa} = \kappa(h) = \left[f'(h)^2 + g'(h)^2\right]^{1/2} \tag{4.5}$$

The material properties $A(\bar{\kappa}, \Omega)$ and $B(\bar{\kappa}, \Omega)$ are then expressed in terms of t_x and t_y by

$$A(\bar{\kappa}, \Omega) = \frac{1}{\bar{\kappa}^2}\left[t_x g'(h) - t_y f'(h)\right], \tag{4.6}$$

$$B(\bar{\kappa}, \Omega) = \frac{1}{\bar{\kappa}^2}\left[t_x f'(h) + t_y g'(h)\right]. \tag{4.7}$$

These expressions are used to calculate the material properties A and B when t_x and t_y have been measured and $f'(h)$, $g'(h)$ are known. When inertial effects are neglected, $f'(h)$ and $g'(h)$ are, (cf. [8]),

$$f'(h) = 0, \qquad g'(h) = a/h, \tag{4.8}$$

so that $\bar{\kappa} = g'(h) = a/h$. Let the material properties in this case by denoted by $A_0(\bar{\kappa}, \Omega)$ and $B_0(\bar{\kappa}, \Omega)$. By (4.6)–(4.8) these are given by

$$A_0(\bar{\kappa}, \Omega) = \frac{h}{a} t_x, \tag{4.9}$$

$$B_0(\bar{\kappa}, \Omega) = \frac{h}{a} t_y. \tag{4.10}$$

Expressions for the relative error in using (4.9) and (4.10) are obtained from (4.3), (4.4), (4.9) and (4.10). These are

$$\frac{A_0 - A}{A} = \frac{h}{a} f' \frac{B}{A} + \left(\frac{h}{a} g' - 1 \right), \tag{4.11}$$

$$\frac{B_0 - B}{B} = -\frac{h}{a} f' \frac{A}{B} + \left(\frac{h}{a} g' - 1 \right), \tag{4.12}$$

in which all quantities are evaluated at $z = h$. Computations show that $|f'|$ is generally very small, so that the first terms on the right hand sides of (4.11) and (4.12) are negligible. Thus, the relative error in using (4.9) and (4.10) to compute A_0 and B_0 depends on how much $g'(h)$ deviates from a/h, (or equivalently, how much $g(z)$ deviates from being a straight line).

Let the following dimensionless variables be introduced: $\hat{z} = z/h$, $\hat{f} = f/a$, $\hat{g} = g/a$ from which it follows that

$$\kappa = \frac{a}{h} \hat{\kappa}, \quad \hat{\kappa}(\hat{z}) = \left[\left(\frac{\mathrm{d}\hat{f}}{\mathrm{d}\hat{z}} \right)^2 + \left(\frac{\mathrm{d}\hat{g}}{\mathrm{d}\hat{z}} \right)^2 \right]^{1/2}. \tag{4.13}$$

Also let $\hat{A}(\hat{\kappa}, \Omega) = A(\kappa, \Omega)/\tilde{G}(\Omega)$ and $\hat{B}(\hat{\kappa}, \Omega) = B(\kappa, \Omega)/\tilde{G}(\Omega)$, where $\tilde{G}(\Omega) = [G_1(\Omega)^2 + G_2(\Omega)^2]^{1/2}$. The boundary value problem (4.1), (4.2) and (2.7) becomes

$$\frac{\mathrm{d}}{\mathrm{d}\hat{z}} \left[\hat{B}(\hat{\kappa}, \Omega) \frac{\mathrm{d}\hat{f}}{\mathrm{d}\hat{z}} + \hat{A}(\hat{\kappa}, \Omega) \frac{\mathrm{d}\hat{g}}{\mathrm{d}\hat{z}} \right] = S^2 \hat{f}(\hat{z}), \tag{4.14}$$

$$\frac{\mathrm{d}}{\mathrm{d}\hat{z}} \left[-\hat{A}(\hat{\kappa}, \Omega) \frac{\mathrm{d}\hat{f}}{\mathrm{d}\hat{z}} + \hat{B}(\hat{\kappa}, \Omega) \frac{\mathrm{d}\hat{g}}{\mathrm{d}\hat{z}} \right] = S^2 \hat{g}(\hat{z}), \tag{4.15}$$

$$\hat{f}(0) = \hat{g}(0) = \hat{f}(1) = 0, \qquad \hat{g}(1) = 1, \tag{4.16}$$

where

$$S^2 = \frac{\rho \Omega^2 h^2}{\tilde{G}(\Omega)}.$$

The dimensionless parameter S represents the ratio of the physical gap length h to a natural length $L = [\tilde{G}(\Omega)/\rho]^{1/2}/\Omega$. Let T_R be a characteristic relaxation time in shear calculated from the relaxation function $G(t)$. Then S can also be written as the product of a Reynold's number $[\rho\Omega h^2/(T_R\tilde{G}(\Omega))]$ and a Deborah number (ΩT_R). For the discussion of the effect of inertia, it is more convenient to regard S in the form $S = h/L$. This natural length appears in the exact analytic solution obtained by Rajagopal and Wineman [9]. When inertia is neglected the natural length becomes infinite and the dimensional solution is

$$f(z) = 0, \qquad g(z) = \frac{a}{h}z. \tag{4.17}$$

When inertial effects are small, the gap is very small compared to L and the solution in [9] differs from (4.17) by terms of $O(S)$. This solution shows that the importance of inertia increases as h increases relative to L. For a given fluid, this occurs when either the gap size h increases or $\tilde{g}(\Omega)^{1/2}/\Omega$ decreases. The latter occurs as Ω increases and $\tilde{G}(\Omega)$ approaches $\tilde{G}(0)$. The solution in [9] shows that the deviation of $g'(h)$ from a/h (or equivalently, the deviation of $g(z)$ from az/h) increases with S, and so do the relative errors in (4.11) and (4.12). In particular, both $f(z)$ and $g(z)$ approach zero in the neighborhood of $z = 0$ and become very steep near $z = \pm h$.

Now consider a class of fluids whose relaxation functions $G^*(s)$ can be expressed in terms of a given relaxation function $G(s)$ by the relation $G^*(s) = G_0 G(s)\, e^{-\alpha s}$. As G_0 decreases or α increases, it follows from (3.16) and (3.17) that $\tilde{G}(\Omega)$ associated with $G^*(s)$ decreases for fixed Ω and so does the zero shear rate viscosity $\eta_0 = \int_0^\infty G^*(s)\, ds$. For such fluids inertial effects become more important.

The Wagner model given in (3.13) displays these characteristics. As κ increases the steady shear rate viscosity and the properties A and B defined in (3.14) and (3.15) decrease for fixed Ω. On the basis of the above discussion it can be expected that the consequence of shear thinning is to enhance the effect of inertia. This is explored in the next sections.

5. Material property functions A and B

Since the material property functions $A(\kappa, \Omega)$ and $B(\kappa, \Omega)$ are non-linear functions of f' and g', the system of eqns. (4.1) and (4.2) must be solved using numerical methods. Any such procedure will require $A(\kappa, \Omega)$ and $B(\kappa, \Omega)$ to be evaluated for a large number of choices of the argument κ. To reduce the cost of computation associated with a large number of evaluations of the integrals in (3.14) and (3.15), $A(\kappa, \Omega)$ and $B(\kappa, \Omega)$ were first

computed for a finite set of values κ_j for a fixed choice of Ω. They were then approximated using a spline interpolation.

The integrals were first written as a summation of subintegrals each over a period of $2\pi/\Omega$. Each subintegral was then evaluated using a 10-point Newton–Cotes formula with an error control algorithm which was developed by the University of Michigan Computing Center. The summations were truncated when the $(N+1)$st subintegral was 10^{-6} times the sum of the first N subintegrals.

Alternate forms of (3.14) and (3.15) can be derived by integration by parts to obtain integrals which are expressed in terms of $G(s)$. In these forms, the derivative of

$$\exp\left[-n\kappa\sqrt{2(1-\cos\Omega s)}\right]\sin\Omega s,$$

which appears in the integral of $A(\kappa, \Omega)$, becomes very large near $s = 2\pi i/\Omega$. Due to this behavior, evaluation of the integral becomes very costly. The derivative of

$$\exp\left[-n\kappa\sqrt{2(1-\cos\Omega s)}\right](1-\cos\Omega s)$$

which appears in the integral of $B(\kappa, \Omega)$ is well behaved.

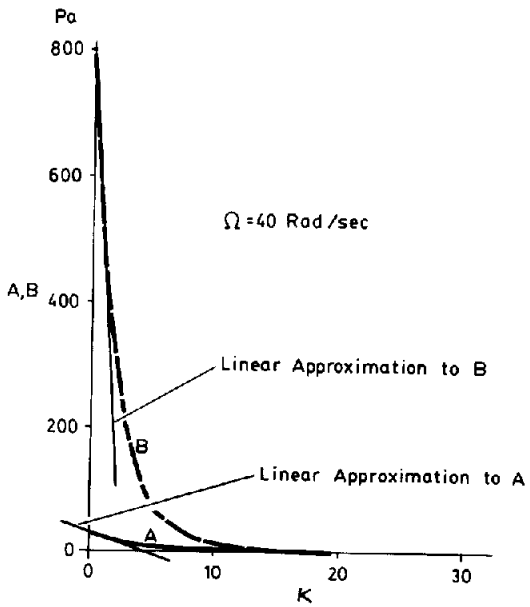

Fig. 2. Plot of $A(\kappa, 40)$ and $B(\kappa, 40)$ vs. κ, with linear approximations on [0,2].

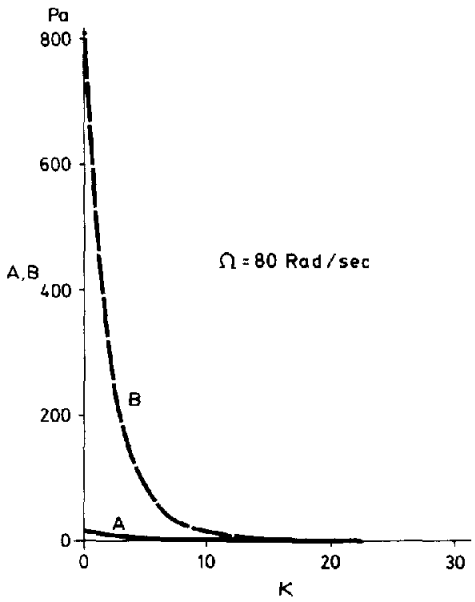

Fig. 3. Plot of $A(\kappa, 80)$ and $B(\kappa, 80)$ vs. κ.

Values for $B(\kappa, \Omega)$ computed using the form in (3.15) involving $\dot{G}(s)$ were compared to values computed using its alternate form involving $G(s)$ which was obtained by integration by parts. Agreement was very good. Thus, $A(\kappa, \Omega)$ was computed using (3.14).

Results for $\Omega = 40$ and 80 rad/s are shown in Figs. 2 and 3. For each Ω, $A(\kappa, \Omega)$ and $B(\kappa, \Omega)$ decay rapidly with increasing κ. This shows the effect of the exponential in the integrand. The material property functions are seen to be nearly linear functions of κ, for $0 \leqslant \kappa \leqslant 2$, so that in this range,

$$A(\kappa, \Omega) \approx A_1(\Omega)\kappa + A_2(\Omega), \tag{5.1}$$

$$B(\kappa, \Omega) \approx B_1(\Omega)\kappa + B_2(\Omega). \tag{5.2}$$

Values for these slopes and intercepts, based on a least squares approximation, are listed in Table 2

TABLE 2

Approximate slopes and intercepts of the material property functions, $A(\kappa, \Omega)$ and $B(\kappa, \Omega)$ on [0,2]

(Rad/s)	$A_1(\Omega)$(Pa)	$A_2(\Omega)$(Pa)	$B_1(\Omega)$(Pa)	$B_2(\Omega)$(Pa)
40	−8.68	31.86	−339.3	799.9
80	−3.79	15.94	−339.2	800.0

6. Method of solution

It can be seen from the exact solution in [9] that as inertial effects become dominant, $f(z)$ and $g(z)$ change more rapidly near $z = \pm h$. For this reason, a Runge–Kutta–Fehlberg method was used (cf. [17]) to solve the system (4.14)–(4.16). The method provides a means of estimating the error and reducing the step size used to control the error. The accuracy of this method is of the order of the step size squared.

Equations (4.14) and (4.15) are not in a form which is appropriate for the use of the Runge–Kutta–Fehlberg method because $\hat{A}(\hat{\kappa}, \Omega)$ and $\hat{B}(\hat{\kappa}, \Omega)$ are non-linear functions of $\mathrm{d}\hat{f}/\mathrm{d}\hat{z}$ and $\mathrm{d}\hat{g}/\mathrm{d}\hat{z}$. However, these equations can be transformed into a system of four first order equations to which the method can be applied. Let $\hat{\sigma}_{xz}$ and $\hat{\sigma}_{yz}$ denote the dimensionless shear stresses

$$\hat{\sigma}_{xz} = \frac{h}{a}\frac{T_{xz}}{\bar{G}(\Omega)}, \qquad \hat{\sigma}_{yz} = \frac{h}{a}\frac{T_{yz}}{\bar{G}(\Omega)}. \tag{6.1}$$

Relations (3.8) and (3.9) can be written in terms of dimensionless quantities as

$$\hat{\sigma}_{xz} = \hat{B}\hat{f}' + \hat{A}\hat{g}' \tag{6.2}$$

$$\hat{\sigma}_{yz} = -\hat{A}\hat{f}' + \hat{B}\hat{g}', \tag{6.3}$$

where the prime now denotes differentiation with respect to $\hat{z}$. Then, by (6.2) and (6.3)

$$\hat{\sigma}^2 = M(\hat{\kappa}, \Omega), \tag{6.4}$$

where $\hat{\sigma}$ is the resultant shear stress, i.e.

$$\hat{\sigma}^2 = \hat{\sigma}_{xz}^2 + \hat{\sigma}_{yz}^2, \tag{6.5}$$

and

$$M(\hat{\kappa}, \Omega) = \hat{\kappa}^2\left[\hat{A}^2(\hat{\kappa}, \Omega) + \hat{B}^2(\hat{\kappa}, \Omega)\right]. \tag{6.6}$$

It is assumed that M is an invertible function of $\hat{\kappa}$ in the domain of interest. Then

$$\hat{\kappa} = M^{-1}(\hat{\sigma}^2, \Omega). \tag{6.7}$$

Let $\hat{A}^*(\hat{\sigma}, \Omega)$ and $\hat{B}^*(\hat{\sigma}, \Omega)$ be defined by the change of variables using (6.7)

$$\hat{A}^*(\hat{\sigma}, \Omega) = \hat{A}\left(M^{-1}(\hat{\sigma}^2, \Omega), \Omega\right), \tag{6.8}$$

$$\hat{B}^*(\hat{\sigma}, \Omega) = \hat{B}\left(M^{-1}(\hat{\sigma}^2, \Omega), \Omega\right). \tag{6.9}$$

Because of the complicated forms of $\hat{A}(\hat{\kappa}, \Omega)$ and $\hat{B}(\hat{\kappa}, \Omega)$, it is not possible to obtain an analytic expression for the inverse in (6.7). When the numerical integration procedure calls for, say, $\hat{A}^*(\hat{\sigma}, \Omega)$ at some value $\hat{\sigma}$, the corresponding value of $\hat{\kappa}$ is determined by numerical solution of the non-linear eqn. (6.4). $\hat{A}^*$ is the evaluation at this $\hat{\kappa}$.

When $n = 0$ in eqn. (3.13), $M(\hat{\kappa}, \Omega)$ reduces to the form $M(\hat{\kappa}, \Omega) = M_0(\Omega)\hat{\kappa}^2$. When $n = 0.29$, $M(\hat{\kappa}, \Omega)$ increases from zero at $\hat{\kappa} = 0$ to a local maximum at some value $\hat{\kappa}_M$, and then decays to zero. It was assumed that when $n = 0.29$, the solution would not differ strongly from the solution when $n = 0$. Thus, in the computations which are discussed in Section 7, it was assumed that the solution would lie on the branch of $M(\hat{\kappa}, \Omega)$ for $0 \leqslant \hat{\kappa} \leqslant \kappa_M$. However, there may be conditions which lead to multiple solutions associated with the use of the branch of $M(\hat{\kappa}, \Omega)$ for $\hat{\kappa} \geqslant \hat{\kappa}_M$.

Finally, solving for $\hat{f}'$ and $\hat{g}'$ from (6.2) and (6.3) and using (6.8) and (6.9), we obtain

$$\frac{\mathrm{d}\hat{f}}{\mathrm{d}\hat{z}} = \left[\hat{B}^*(\hat{\sigma}, \Omega)\hat{\sigma}_{xz} - \hat{A}^*(\hat{\sigma}, \Omega)\hat{\sigma}_{yz}\right]/\Delta, \tag{6.10}$$

$$\frac{\mathrm{d}\hat{g}}{\mathrm{d}\hat{z}} = \left[\hat{A}^*(\hat{\sigma}, \Omega)\hat{\sigma}_{xz} + \hat{B}^*(\hat{\sigma}, \Omega)\hat{\sigma}_{yz}\right]/\Delta, \tag{6.11}$$

where

$$\Delta = \hat{A}^*(\hat{\sigma}, \Omega)^2 + \hat{B}^*(\hat{\sigma}, \Omega)^2. \tag{6.12}$$

Equations (6.10) and (6.11) are two first order ordinary differential equations for $\hat{f}$, $\hat{g}$, $\hat{\sigma}_{xz}$, $\hat{\sigma}_{yz}$. The remaining two equations are obtained by substituting (6.2) and (6.3) into (4.14) and (4.15) to give

$$\frac{\mathrm{d}}{\mathrm{d}\hat{z}}\hat{\sigma}_{xz} = S^2\hat{f}, \tag{6.13}$$

$$\frac{\mathrm{d}}{\mathrm{d}z}\hat{\sigma}_{yz} = S^2\hat{g}. \tag{6.14}$$

Equations (6.10)–(6.14) are in the standard form for the application of the Runga–Kutta–Fehlberg method. These equations, together with the boundary conditions (4.16), define a two point boundary value problem. The method of integration of (6.10)–(6.14) requires values for $\hat{\sigma}_{xz}(0)$ and $\hat{\sigma}_{yz}(0)$, which are not known. Let vectors $\{b\}$ and $\{e\}$ be defined as

$$\{b\} = \begin{Bmatrix} \hat{\sigma}_{xz}(0) \\ \hat{\sigma}_{yz}(0) \end{Bmatrix}, \qquad \{e\} = \begin{Bmatrix} f(1) \\ g(1) - 1 \end{Bmatrix}. \tag{6.15}$$

There is some function $[D]$ such that

$$[D(\{b\})] = \{e\}. \tag{6.16}$$

The correct starting value $\{b^*\}$ is a zero of $[D]$. The starting value $\{b^*\}$ is determined by the quasi-Newton iteration procedure

$$\{b_{i+1}\} = \{b_i\} + [B_i]\{e_i\}, \tag{6.17}$$

in which $[B_i]$ is obtained by first using Broyden's method [18] to construct a rank one update to the Jacobian as an approximation to the Jacobian, and then applying the method of Sherman and Morrison [17] to directly compute the inverse of this matrix from the original inverse and the updating vector.

7. Numerical results

The parameters chosen for this study were typical of those reported in the literature on the experimental application of the orthogonal rheometer [1]. Results are presented for the plate separation $h = 0.01$ m and offset ratio $a/h = 0.1$. Results for a larger set of parameters can be found in [19]. The values of the dimensionless parameter S defined in (4.16) are $S = 0.424$ and 0.848 for $\Omega = 40$ rad/s and 80 rad/s, respectively.

The numerical solution of the boundary value problem (4.14)–(4.16) was compared with the exact analytical solution of Rajagopal and Wineman [9] for the case where the material property functions are independent of κ. For plate angular velocities $\Omega = 40$ rad/s and $\Omega = 80$ rad/s, there was agreement to at least 5 significant digits. In all of the computations to be discussed, it was found that $\hat{f}$ never exceeded 10^{-5}.

It will be instructive to first consider the case in which the material property functions are independent of $\hat{\kappa}$ (i.e., $n = 0$ in (3.13)). A plot of $\hat{g}(\hat{z})$ for several values of Ω is shown in Fig. 4. The straight line represents the

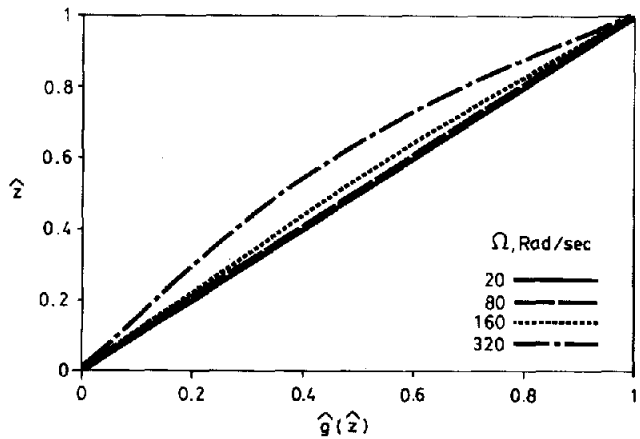

Fig. 4. Plots of $\hat{g}(\hat{z})$ v. $\hat{z}$ for A, B independent of κ, $h = 0.01$ m, $a/h = 0.1$.

solution $\hat{g} = \hat{z}$, when inertia is neglected, (see (4.17)). Deviation from this solution is very small even at $\Omega = 80$ rad/s. Inertia causes $\hat{g}'$ to decrease near $\hat{z} = 0$ and to increase near $\hat{z} = 1$.

A convenient quantity for showing the effect of inertia on the stresses in the fluid is the dimensionless resultant shear stress $\hat{\sigma}$ which is related to the dimensionless shear amplitude $\hat{\kappa}$ and material properties in (6.4)–(6.6). By (3.14)–(3.17), and the non-dimensionalization introduced following (4.13), $\hat{\sigma} = \hat{\kappa}$ when material properties $A(\kappa, \Omega)$ and $B(\kappa, \Omega)$ are independent of κ. Furthermore, $\mathrm{d}\hat{f}/\mathrm{d}\hat{z}$ is negligible so that $\hat{\sigma} \approx \mathrm{d}\hat{g}/\mathrm{d}\hat{z}$. Figure 5 shows $\hat{\sigma}(\hat{z})$ for various values of Ω. The vertical line corresponds to the inertialess case $\hat{\sigma} = 1$. As Ω increases there is increased deviation of $\hat{\sigma}$ or $\mathrm{d}\hat{g}/\mathrm{d}\hat{z}$ from the inertialess solution especially at $\hat{z} = 1$, i.e., at the plates of the orthogonal rheometer. Consequently, by (4.11) and (4.12), there is increased error in the use of (4.9) and (4.10) where inertia is neglected to determine the material properties from experimental data. Table 3 lists dimensional values of the material property functions and the relative error for these calculations. The relative error increases rapidly with Ω.

Results for the case in which the material properties depend on $\hat{\kappa}$, ($n = 0.29$ in (3.13)) were calculated for $\Omega = 40$ and 80 rad/s. Consider first the case in which inertia is neglected. In this case, $\hat{g} = \hat{z}$ and it follows from (6.4), (6.6), (4.13), and (4.17) that

$$\hat{\sigma} = \left[A(a/h, \Omega)^2 + B(a/h, \Omega)^2\right]^{1/2} / \tilde{G}(\Omega). \tag{7.1}$$

For each value of Ω, this represents a vertical line in Fig. 6. For the material model under consideration, the values of this expression are about 0.96 for

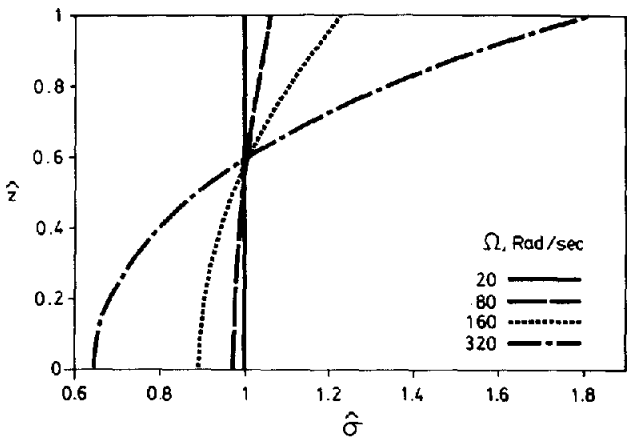

Fig. 5. Plot of $\hat{\sigma}$ vs. $\hat{z}$ for A, B independent of κ, $h = 0.01$ m, $a/h = 0.1$.

TABLE 3

Values of material moduli calculated with and without accounting for inertia (A, B—with Inertia; A_0, B_0—without Inertia; ($h/a = 0.1$, $h = 0.01$ m)

	Ω	A	A_0	$\frac{A_0 - A}{A}$	B	B_0	$\frac{B_0 - B}{B}$
I.	20	66.175	66.175	–	800	809.45	0.3×10^{-3}
	40	31.861	31.862	3×10^{-5}	800	811.9	0.015
	80	15.935	15.936	6×10^{-5}	800	847.93	0.059
	160	2.433	2.436	10^{-3}	800	983.37	0.229
II.	40	30.979	30.994	4×10^{-4}	765.38	777.89	0.016
	80	15.531	15.569	2×10^{-3}	763.76	813.34	0.065
III.	40	30.094	30.127	1.1×10^{-3}	730.71	743.88	0.018
	80	15.123	15.191	4×10^{-3}	727.12	779.24	0.072
IV.	40	21.511	21.534	1.1×10^{-3}	525.17	537.94	0.024
	80	10.784	10.839	5×10^{-3}	522.73	573.03	0.0962

Ω in rad/sec, A, A_0, B, B_0 in Pa
I. A, B independent of κ
II. Actual material response
III. A, B linear in κ, slope $\hat{B}_1 = -680$, $\hat{B}_2 = B_2^*$
IV. A, B linear in κ, intercept $\hat{B}_2 = 560$, $\hat{B}_1 = B_1^*$.

$a/h = 0.1$, $\Omega = 40$ rad/s and $\Omega = 80$ rad/s. Plots of $\hat{g}(\hat{z})$, when inertia is included, are similar to those shown in Fig. 4 and are omitted here due to lack of space. The graphs of $\hat{g}(\hat{z})$, with and without inertia, do not appear to

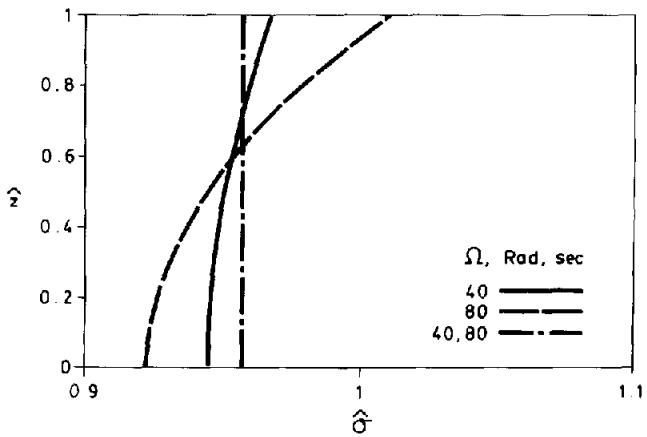

Fig. 6. Plot of $\hat{\sigma}$ vs. $\hat{z}$ for actual A, B dependence on κ. $h = 0.01$ m, $a/h = 0.1$.

differ by very much. The differences are probably not large enough to be detectable by experimental optical methods. Yet the spatial variation of $\mathrm{d}\hat{g}/\mathrm{d}\hat{z}$ cannot be ignored. The combined influence of the spatial variation of $\mathrm{d}\hat{g}/\mathrm{d}\hat{z}$, and hence $\hat{\kappa}$, and the rapid decrease of A and B with shear amplitude cause significant deviation of $\hat{\sigma}$ from the inertialess case, as is shown in Fig. 6. This deviation increases as Ω increases. This is also seen in Table 3 which lists the dimensional values of the material property functions and the relative error. The relative error is increased by shear thinning. This can be explained by considering (6.4), (6.6) and (7.1) at $\hat{z} = 1$, where material properties are evaluated. The value of $\hat{\kappa}$, when inertia is considered, is greater than $\hat{\kappa} = 1$, when inertia is neglected. Because of shear thinning, the coefficient of $\hat{\kappa}$, with inertia, is smaller than in (7.1), where inertia is neglected.

As was discussed in section 5, the material property functions A and B can be approximated very closely for $0 \leqslant \kappa \leqslant 2$ by the linear functions (5.1) and (5.2), respectively. These expressions were used in a study of the dependence of the solution on slopes A_1 and B_1 and intercepts A_2 and B_2. Since B is significantly greater than A for the rotation rates considered, it was assumed that $B(\kappa, \Omega)$ has a greater effect on the solution. The variation of $A(\kappa, \Omega)$ was thus related to the variation of $B(\kappa, \Omega)$ by writing

$$B(\kappa, \Omega) = \hat{B}_1 \kappa + \hat{B}_2, \tag{7.2}$$

$$A(\kappa, \Omega) = a_1 \hat{B}_1 \kappa + a_2 \hat{B}_2. \tag{7.3}$$

In (7.2) and (7.3) $\hat{B}_i$ are the independent variables for the study and coefficients a_i are defined as

$$a_i = A_i^*(\Omega)/B_i^*(\Omega), \qquad i = 1, 2, \tag{7.4}$$

where A_i^* and B_i^* are the best fit values listed in Table 2. Results are shown for $\Omega = 80$ rad/s.

Numerical results obtained using (7.2) and (7.3) with $\hat{A}_i = A_i^*$, $\hat{B}_i = B_i^*$ were very close to the numerical results obtained for the actual material model. By varying $\hat{B}_1$, one can study the effect of changing the rate of shear thinning parameter n in (3.14) and (3.15). By varying $\hat{B}_2$, one can study the effect of changing the zero shear strain amplitude values of A and B, which is equivalent to scaling the relaxation function $G(t)$.

Graphs of $\hat{g}(\hat{z})$ are again omitted for brevity. The earlier comparison of $\hat{g}(\hat{z})$ with the straight line in the inertialess case also applies here. The deviation of $\hat{g}(\hat{z})$ from linearity increases as the slope magnitude $|\hat{B}_1|$ increases or as the intercept $\hat{B}_2$ decreases. The deviation of $\hat{g}$ from linearity is much more sensitive to changes in the intercept parameter $\hat{B}_2$. Figure 7 shows the effect of varying the slope parameter $\hat{B}_1$ for fixed intercept

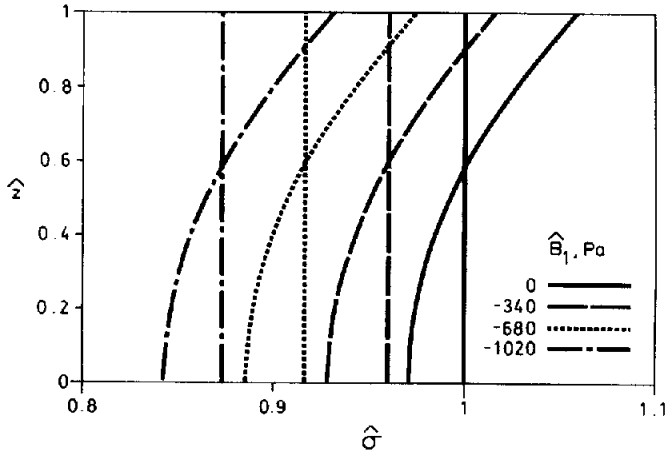

Fig. 7. Plot of $\hat{\sigma}$ vs. $\hat{z}$ for A, B linearly dependent on κ. $h = 0.01$ m, $a/h = 0.1$, $\Omega = 80$ rad/s, $\hat{B}_2 = B_2^*$ and various slopes $\hat{B}_1$.

parameter $\hat{B}_2 = B_2^*$. Figure 8 shows the effect of varying the intercept parameter $\hat{B}_2$ for fixed $\hat{B}_1 = B_1^*$. The curves in these figures should be compared with that for $\Omega = 80$ rad/s in fig. 6. An increase in the slope parameter $|\hat{B}_1|$ appears to have very little effect on $d\hat{g}/d\hat{z}$ and the shear amplitude $\hat{\kappa}$. The dominant effect is to reduce the value of the coefficient of $\hat{\kappa}$ in (6.6) and thereby scale down the size of $\hat{\sigma}$. On the other hand, reducing the intercept $\hat{B}_2$ causes $d\hat{g}/d\hat{z}$ to increase near $\hat{z} = 1$ and decrease near

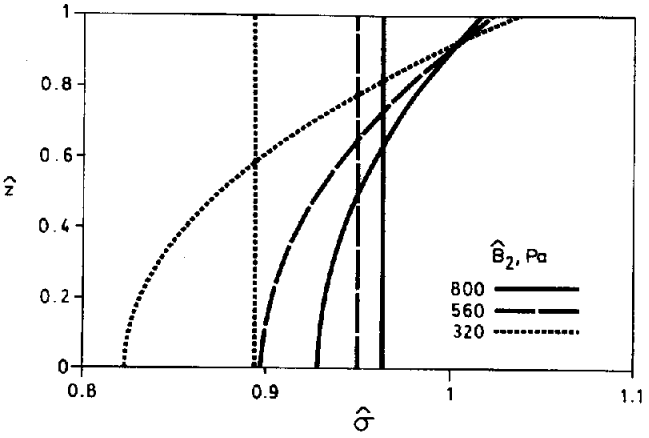

Fig. 8. Plot of $\hat{\sigma}$ vs. $\hat{z}$ for A, B linearly dependent on κ. $h = 0.01$ m, $a/h = 0.1$, $\Omega = 80$ rad/s. $\hat{B}_1 = B_1^*$ and various intercepts $\hat{B}_2$.

$\hat{z} = 0$. This results in a complete change in the shape of the graph of $\hat{\sigma}$. As seen in Table 3, the relative error is increased by reducing the zero shear magnitudes of A and B, or if the rate of shear thinning is increased.

Conclusions

The conclusions to be drawn from this study apply only to the particular fluid model considered here. However, the study does provide substantial insight into the combined effects of inertia and shear thinning in an orthogonal rheometer which can be expected in similar fluid models. The values of, Ω, a/h and h used in this study are representative of the upper range of values which have appeared in the experimental literature. For these values, the results show that inertia and shear thinning effects are becoming important. For larger values of these parameters, inertia and shear thinning cannot be neglected. Their importance is amplified as the rate of shear thinning increases or as the moduli A and B are scaled down in magnitude.

References

1 B. Maxwell and R.P. Chartoff, Trans. Soc. Rheol., 9 (1965) 41.
2 L.L. Blyler and S.J. Kurtz, J. Appl. Poly. Sci., 11 (1967) 127.
3 C. Goldstein and W.R. Schowalter, Trans. Soc. Rheol., 19 (1975) 1.
4 K.R. Rajagopal, Arch. Rat. Mech. Anal., 79 (1982) 39.
5 T.N. Abbott and K. Walters, J. Fluid Mech., 40 (1970) 205.
6 C. Truesdell and W. Noll, The Nonlinear Field Theories of Mechanics. In: S. Flugge (Ed.), Encyl. of Physics Vol. III/3, Springer-Verlag, New York, 1965.
7 K.R. Rajagopal, J. Non-Newtonian Fluid Mech., 9, (1981) 185.
8 J.D. Goddard, Quart. Appl. Math., 41 (1983) 107.
9 K.R. Rajagopal and A.S. Wineman, J. Rheology, 27 (1983) 509.
10 A.S. Lodge, Elastic Liquids. Academic Press, New York, 1964.
11 K.R. Rajagopal, M. Renardy, Y. Renardy, A.S. Wineman, Rheol. Acta (to appear).
12 Berker, R., Int. J. Eng. Sci., 20 (1982) 217.
13 A. Kaye, College of Aeronautics, Note No. 134, Cranfield, 1962.
14 B. Bernstein, E.A. Kearsley and L.J. Zapas, Trans. Soc. Rheol., 7 (1963) 391.
15 M.H. Wagner, Rheol. Acta., 15 (1976) 133.
16 L.J. Zapas, personal communication.
17 B.L. Burden, J.D. Faires and A.C. Reynolds, Numerical Analysis. Prindle, Weber & Schmidt, Boston, Mass., 1981.
18 D.G. Luenberger, Introduction to Linear and Nonlinear Programming. Addison-Wesley Publishing Co., Reading, Mass., 1973.
19 M.V. Bower, Numerical Simulation of Viscoelastic Flows of Polymer Fluids. University of Michigan Ph.D. Dissertation, 1985.